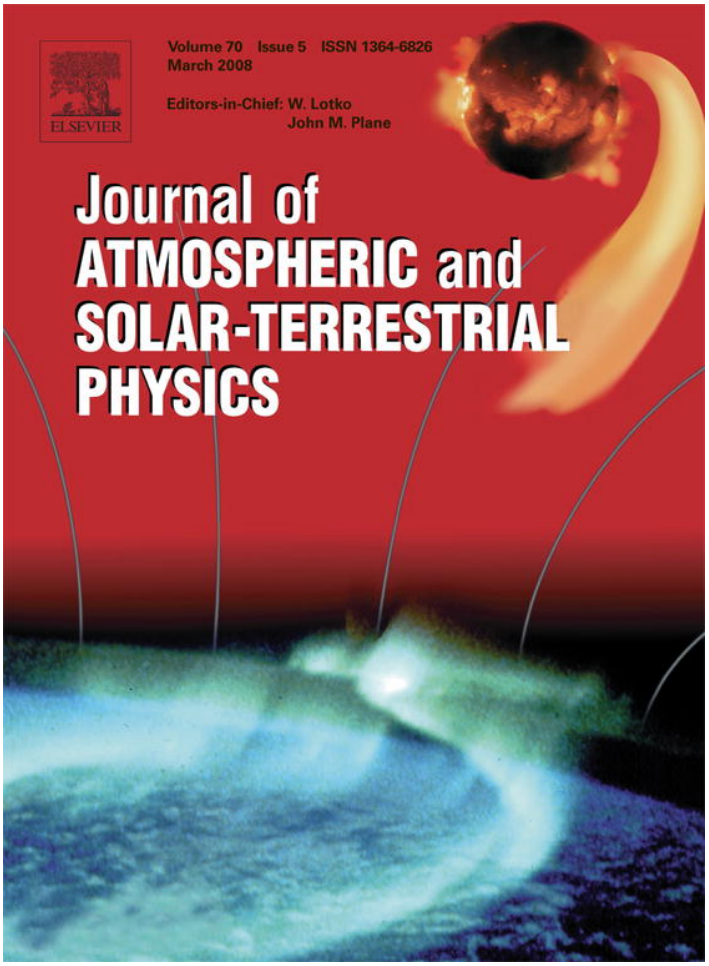

ELSEVIER

Journal of Atmospheric and Solar-Terrestrial Physics 70 (2008) 774–793

Journal of ATMOSPHERIC AND SOLAR-TERRESTRIAL PHYSICS

www.elsevier.com/locate/jastp

The JB2006 empirical thermospheric density model

Bruce R. Bowman[a,*], W. Kent Tobiska[b,1], Frank A. Marcos[c,2], Cesar Valladares[d,3]

[a]*Air Force Space Command, Space Analysis/A9AC, 250 S. Peterson Boulevard, Suite 116, Peterson AFB, CO 80914, USA*
[b]*Space Environment Technologies, 1676 Palisades Dr., Pacific Palisades, CA 90272, USA*
[c]*Air Force Research Laboratory, Space Vehicles Directorate, AFRL /VSBXT, 29 Randolph Road, Hanscom AFB, MA 01731-3010, USA*
[d]*Boston College, Institute for Space Research, 140 Commonwealth Avenue, St. Clement's Hall 410, Chestnut Hill, MA 02467-3862, USA*

Received 6 July 2007; received in revised form 17 September 2007; accepted 7 October 2007
Available online 23 October 2007

Abstract

A new empirical atmospheric density model is developed using the CIRA72 (Jacchia 71) model as the basis for the diffusion equations. New solar indices based on orbit-based sensor data are used for the solar irradiances in the extreme and far ultraviolet wavelengths. New exospheric temperature and semiannual density equations are employed to represent the major thermospheric density variations. Temperature correction equations are also developed for diurnal and latitudinal effects, and finally density correction factors are used for model corrections required at high altitude (1500–4000 km). The new model, Jacchia–Bowman 2006, is validated through comparisons of accurate daily density drag data previously computed for numerous satellites. For 400 km altitude the standard deviation of 16% for the standard Jacchia model is reduced to 10% for the new JB2006 model for periods of low geomagnetic storm activity.

Keywords: Thermosphere; Thermosphere models; Solar EUV; Neutral density; Semiannual variation

1. Introduction

Density model errors on the order of 15–20% one standard deviation have been recognized for all empirical models (Marcos, 1990) developed since the mid-1960s. These large-density standard deviations correspond to maximum density errors of approximately 40–60% as observed in satellite drag data. There are two main reasons for these consistently large values. One is the result of not modeling the semiannual density variation (Bowman, 2004) as a function of solar activity and the other results from not modeling the full thermospheric heating from solar ultraviolet (UV) radiation. Geomagnetic storms provide episodic, and overall smaller, contributions to the standard deviation. All previous empirical atmospheric models (Jacchia, 1970, 1971, 1977; Hedin 1977, 1983, 1991) have used the F_{10} and 81-day centered average $\bar{F}_{10}$ proxies as representative of the solar UV heating. However, the unmodeled errors derived from satellite drag data, as displayed in Fig. 1 for 1999, all show very large density errors with approximately 27-day periods, representing one solar rotation

*Corresponding author. Tel.: +1 719 556 3710.
E-mail addresses: bruce.bowman@peterson.af.mil (B.R. Bowman), ktobiska@spacenvironment.net (W. Kent Tobiska), frank.marcos@hanscom.af.mil (F.A. Marcos), valladar@bc.edu (C. Valladares).
[1]Tel.: +1 310 573 4185 (office); fax: +1 310 454 9665.
[2]Tel.: +1 781 377 3037.
[3]Tel.: +1 617 552 8789.

1364-6826/$ - see front matter © 2007 Elsevier Ltd. All rights reserved.
doi:10.1016/j.jastp.2007.10.002

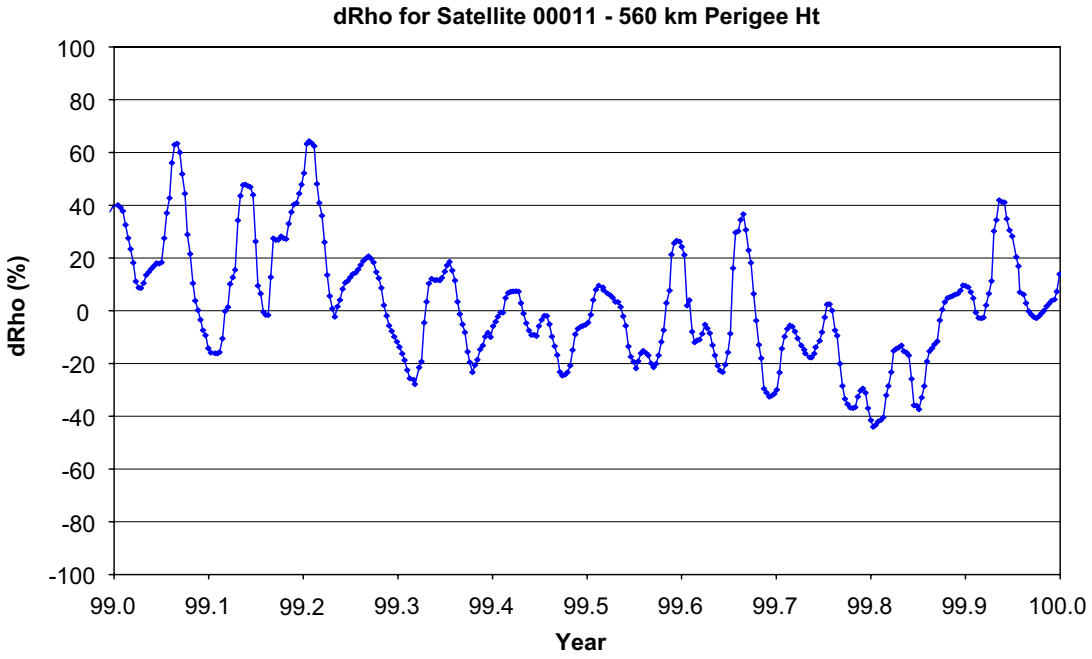

Fig. 1. Density errors, dρ, from Jacchia 70 during 1999 from analysis of the ballistic coefficient (B) values obtained from the orbit fits of the spherical satellite 00011 with a perigee height of 560 km.

cycle. These errors are the result of not fully modeling the UV radiation effects on the thermosphere, which have a one solar rotation periodicity. The purpose of this paper is to describe a new atmospheric model that incorporates new solar indices and a new semiannual density model plus other corrections to the Jacchia model.

The basis of the new Jacchia–Bowman JB2006 model is the CIRA72 (COSPAR, 1972) model atmosphere. The CIRA72 model integrates the diffusion equations using the Jacchia (1971) temperature formulation to compute density values for an input geographical location and solar conditions. The CIRA72 model was first converted to a CIRA "70" model by replacing the CIRA72 equations with equations from the Jacchia 70 model. This was done because the model corrections, for altitudes below 1000 km, obtained for temperature and density are based on the Jacchia (1970) model, not the Jacchia (1971) model used in CIRA72. New semiannual density equations (Bowman, 2004) were developed to replace the Jacchia formulation. New global nighttime minimum exospheric temperature equations (Bowman et al., 2006), using new solar indices, replaced Jacchia's T_c equation. In addition, several other equations to correct errors in the diurnal (local solar time) modeling were also incorporated. Finally, new density factors were incorporated to correct model errors at altitudes from 1000 to 4000 km. All of these new equations and model corrections are discussed in the sections that follow.

2. Data reduction

The density data used to develop the new model equations are very accurate daily values (Bowman et al., 2004) obtained from drag analysis of numerous satellites with perigee altitudes of 175–1100 km. Daily temperature corrections to the US Air Force High Accuracy Satellite Drag Model's (HASDM) (Storz et al., 2002) modified Jacchia (1970) atmospheric model were obtained on the satellites throughout the period 1978–2004. Approximately 120,000 daily temperature values were computed using a special energy dissipation rate (EDR) method (Bowman et al., 2004), where radar and optical observations are fit with special orbit perturbations. For each satellite tracked from 1978 through 2004 approximately 100,000 radar and optical observations were available for the special perturbation orbit fitting. A differential orbit correction program was used to fit the observations to obtain the standard 6 Keplerian elements plus the ballistic coefficient. "True" ballistic coefficients (Bowman, 2002) were then used with the observed daily temperature corrections to obtain daily density values. The daily density computation was

validated (Bowman et al., 2004) by comparing historical daily density values computed for the last 30 years for over 30 satellites. The accuracy of the density values was determined from comparisons of geographically overlapping perigee location data, with over 8500 pairs of density values used in the comparisons. The density errors were found to be less than 4% overall, with errors on the order of 2% for values covering the latest solar maximum.

3. Global nighttime minimum exospheric temperature

The variations in the UV solar radiation that heats the earth's thermosphere consist of two components, one related to solar rotational modulation of active region emission and the other to long-term evolution of the main solar magnetic field (Jacchia, 1971). The passage of active regions across the disk during a solar rotation period produces irradiance variations of approximately 27 days, while the main solar magnetic field evolution produces irradiance variations over approximately 11 years. The 10.7-cm solar flux, $F10.7$ (designated as F_{10} in this paper), has in the past been used to represent these effects. However, new solar indices have been recently (Bowman et al., 2006) used to compute better density variation correlations with UV radiation covering the entire far UV (FUV) as well as the extreme UV (EUV) wavelengths.

In determining a new T_c temperature equation with the new solar indices the density values were converted into daily T_c temperature values using the Jacchia 70 empirical atmospheric density model (Jacchia, 1970). To obtain accurate T_c values the large semiannual density variations had to be correctly modeled. A major density variation, aside from the 11-year and 27-day solar heating effect, is the semiannual change. This can be as large as 250% from a July minimum to an October maximum during solar maximum years, and as small as 60% from July to October during solar minimum years at 600 km (Bowman, 2004). The semiannual variation was computed on a yearly basis from the previously derived density data (Bowman, 2004). Jacchia's 70 model equation was then replaced using these observed semiannual yearly variations. A smaller correction to Jacchia's model was also made for the observed errors in the latitude and local solar time density variations. From these different model corrections an accurate T_c value, due almost entirely to solar heating, was obtained.

The solar UV absorption in the thermosphere was analyzed to determine what new solar indices were required for the new temperature equation development. Fig. 2 is a plot of the altitude at which the

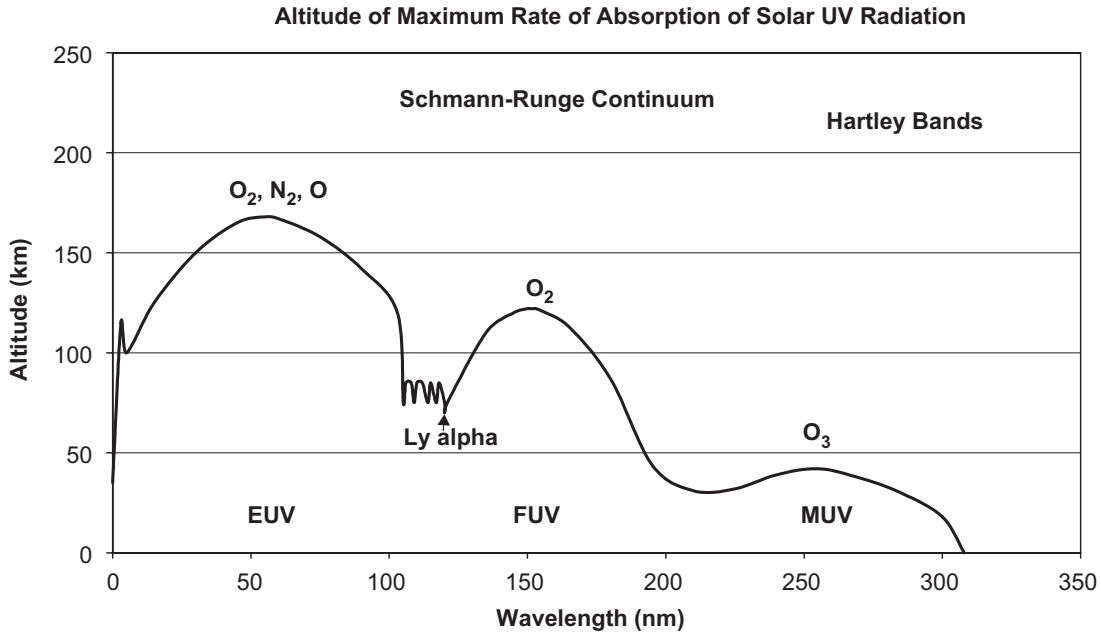

Fig. 2. The altitude of the maximum rate of absorption of solar ultraviolet radiation as a function of solar spectrum wavelength. EUV—extreme ultraviolet, FUV—far ultraviolet, and MUV—mid-ultraviolet region. The relevant atomic/molecular species for absorption are also listed. Figure adapted from Jursa (1985).

maximum absorption rate of solar UV radiation occurs as a function of wavelength (Jursa, 1985). The solar index F_{10} is really a proxy index because it is measured at a 10.7-cm wavelength, which is not a direct measure of any UV radiation. Direct UV heating indices were recently developed that represent the extreme (EUV), far (FUV), and mid (MUV) solar UV radiation. Fig. 2 suggests that, besides an EUV index, an FUV index needs to be considered to capture most of the potential UV heating of the thermosphere.

Based on the previous solar indices analysis (Bowman et al., 2006), the daily indices selected for this model development include F_{10}, S_{10}, and Mg_{10}.

F_{10}: The 10.7-cm solar radio flux, F_{10}, is produced daily by the Canadian National Research Council's Herzberg Institute of Astrophysics at its ground-based Dominion Radio Astrophysical Observatory located in Penticton, British Columbia. The physical units of F_{10} are $W\,m^{-2}\,Hz^{-1}$ and more conveniently expressed in solar flux units ($1\,sfu = 1\times 10^{-22}\,W\,m^{-2}\,Hz^{-1}$). For example, a 10.7-cm radio emission of $150\times 10^{-22}\,W\,m^{-2}\,Hz^{-1}$ is simply referred to as $F_{10} = 150\,sfu$. A running 81-day centered smoothed set of values using the moving boxcar method was created, and these data are referred to as $\bar{F}_{10}$. Linear regression with daily F_{10} has been used to scale and report all other solar indices in units of sfu.

S_{10}: The NASA/ESA Solar and Heliospheric Observatory (SOHO) research satellite operates in a halo orbit at the Lagrange Point 1 (L1) on the Earth–Sun line, approximately 1.5 million kilometers from the Earth. One of the instruments on SOHO is the solar extreme-UV monitor (SEM) that has been measuring the 26–34 nm solar EUV emission since launch in December 1995. This integrated 26–34 nm emission has been normalized and converted to sfu through linear regression with F_{10}, producing the new index S_{10}. The broadband (wavelength integrated) SEM 26–34 nm irradiances are EUV line emissions dominated by the chromospheric He II line at 30.4 nm with contributions from other chromospheric and coronal lines. This energy principally comes from solar active regions.

Mg_{10}: The NOAA series of operational satellites, e.g., NOAA 16 and NOAA 17, host the solar backscatter UV (SBUV) spectrometer that has the objective of monitoring ozone in the Earth's lower atmosphere. In its discrete operating mode, a diffuser screen is placed in front of the instrument's aperture in order to scatter solar MUV radiation near 280 nm into the instrument. This solar spectral region contains both photospheric continuum and chromospheric line emissions. The chromospheric Mg II h and k lines at 279.56 and 280.27 nm, respectively, and the weakly varying photospheric wings (or continuum longward and shortward of the core line emission), are operationally observed by the instrument. The Mg II core-to-wing ratio (cwr) is calculated between the variable lines and nearly non-varying wings. The result is a measure of chromospheric and some photospheric solar active region activity independent of instrument sensitivity change through time, and is referred to as the Mg II cwr, which is provided daily by NOAA Space Environment Center (SEC) (Viereck et al., 2001). The Mg II cwr has been used in a linear regression with F_{10} to derive the Mg_{10} index in sfu.

3.1. T_c temperature equation

The solution of the best T_c equation was obtained using numerous satellites for the years from 1996 through 2004 when all new solar indices were available. The resulting equation is

$$T_c = 379.0 + 3.353\bar{F}_{10} + 0.358\Delta F_{10} + 2.094\Delta S_{10} + 0.343\Delta Mg_{10}. \quad (1)$$

The $\bar{F}_{10}$ represents the 81-day centered average value of the F_{10} index. The delta values (ΔF_{10}, ΔS_{10}, ΔMg_{10}) represent the difference of the daily and 81-day centered average value of each index. The 81-day (3-solar rotation period) centered value was determined to be the best long-term average to use. Table 1 below shows the results of using a 2, 3, and 4 solar rotation period for the centered indices.

Table 1
RMS values are listed for the T_c fits based on using 54-, 81-, and 108-day centered average values for F_{10}, S_{10}, and Mg_{10}

Run	RMS (dT_c (deg.))	Average
1	20.2	54-day centered
2	19.7	81-day centered
3	21.5	108-day centered
		81-day centered
4	19.7	F_{10}
5	30.5	S_{10}
6	41.6	Mg_{10}

Also listed are the RMS results using F_{10}, S_{10}, or Mg_{10} 81-day centered averages to represent the 11-year solar variability.

To avoid increases in T_c due to geomagnetic storms, all daily data with the geomagnetic index $a_p > 25$ were rejected. This meant that if a solar index required a lag time of 5 days, each of the 5 days prior to the current time had to have $a_p < 25$ for the current daily density data to be used.

It was determined (Bowman et al., 2006) that a lag time of 1 day was the best to use for the F_{10} and S_{10} indices. However, for using the Mg_{10} index the analysis initially centered on using an index E_{SRC} representing the FUV solar radiation from the Schumann–Runge continuum shown in Fig. 2. From the analysis it was determined that the Mg_{10} index could be used as an excellent proxy for the real FUV E_{SRC} index. The best time lag determined for both E_{SRC} and Mg_{10} corresponded to a 5-day lag, which was used in determining the new T_c equation above.

3.2. 11-Year cycle temperature fits

Table 1 lists the results of using 2, 3, and 4 solar rotation centered periods for the long-term averages of F_{10}, S_{10}, and Mg_{10} indices. Use of the 3-solar rotation period produces the best root mean square (RMS) average.

Table 1 also lists the results of using 81-day centered values of F_{10}, S_{10}, or Mg_{10} for the representation of the long-term 11-year solar cycle variation. The customary index in use for all previous models has been $\bar{F}_{10}$. In the analysis the 81-day centered S_{10}, and then the Mg_{10}, values were used to replace the $\bar{F}_{10}$ value to represent the long-term effects. Using the $\bar{F}_{10}$ value is significantly better than using either of the other long-term indices.

3.3. Density comparisons

The testing of the new T_c equation was done by placing the new Eq. (1) into the Jacchia 70 atmospheric model, along with the real observed yearly semiannual variations. The new diurnal and latitudinal corrections described in Section 5 were also included. This was then used to compute new ballistic coefficient (DB) variations for the spherical satellite 12 388 at a 400-km perigee altitude. Any unmodeled density variations are aliased into the B solution during the orbit determination process. Fig. 3 shows the results of the recomputed DB variations for 2000. The figure shows a marked improvement in reducing the DB variations with respect to the 27-day solar rotation period.

4. Semiannual density variation

The semiannual density variation was first discovered by Paetzold and Zschorner (1961).

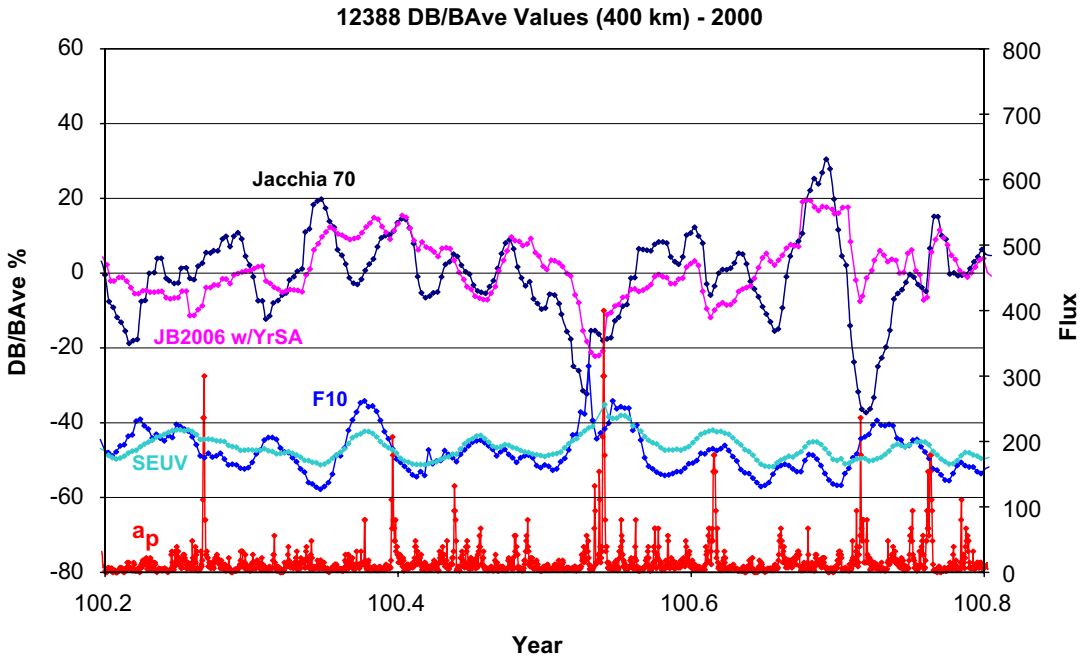

Fig. 3. The delta ballistic coefficient (DB) variations are listed for satellite 12388 for a time period during 2000. The Jacchia data are based on orbit corrections using the original Jacchia 70 model with the observed 2000 semiannual applied. The JB2006 data use the new complete T_c Eq. (1) with the observed 2000 semiannual variation applied. The indices F_{10}, S_{10}, and a_p are also plotted.

They observed a global density variation from analysis of satellite drag data, which showed 6-month periodicity maximum occurring in April and October, and minimum occurring in January and July.

For the new JB2006 model the semiannual variations were computed (Bowman, 2004) first by differencing the real daily density values with density values obtained from the Jacchia model without applying Jacchia's semiannual equations. For a perfect model the resulting differences would only contain the observed semiannual variation. Fig. 4 shows examples of the individual density differences obtained from the data. Also shown are Jacchia's semiannual density variation and a Fourier series fitted to smoothed density difference values. This Fourier function is discussed in detail below. As can be observed in the figure, there is a very large unmodeled 27-day variation in the difference values. Therefore, it was decided to smooth the values with a 28-day moving filter. The resulting values would then produce a smoother fit with the Fourier series.

It is interesting to note how the semiannual variation changes with height and time. Fig. 4 shows the variation during a year near solar maximum (2002). The semiannual amplitude is measured from the yearly minimum, normally occurring in July, to the yearly maximum, normally in October. During solar maximum, the semiannual variation can be as small as 30% at 220 km, and as large as 250% near 800 km. During solar minimum, the maximum variation near 800 km is only 60%. Thus, there is a major difference in amplitudes of the yearly variation from solar minimum to solar maximum, unlike Jacchia's model, which maintains constant amplitude from year to year.

4.1. Semiannual density variation function

Jacchia (1971) represented the semiannual density variation in the form

$$\Delta_{SA} \log_{10} \rho = F(z)G(t), \tag{2}$$

where $F(z)$ represents the variation amplitude (i.e. the difference in $\log_{10}$ density between the principal minimum normally in July and the principle maximum normally in October) as a function of altitude and $G(t)$ represents the average density variation as a function of time in which the amplitude has been normalized to 1.

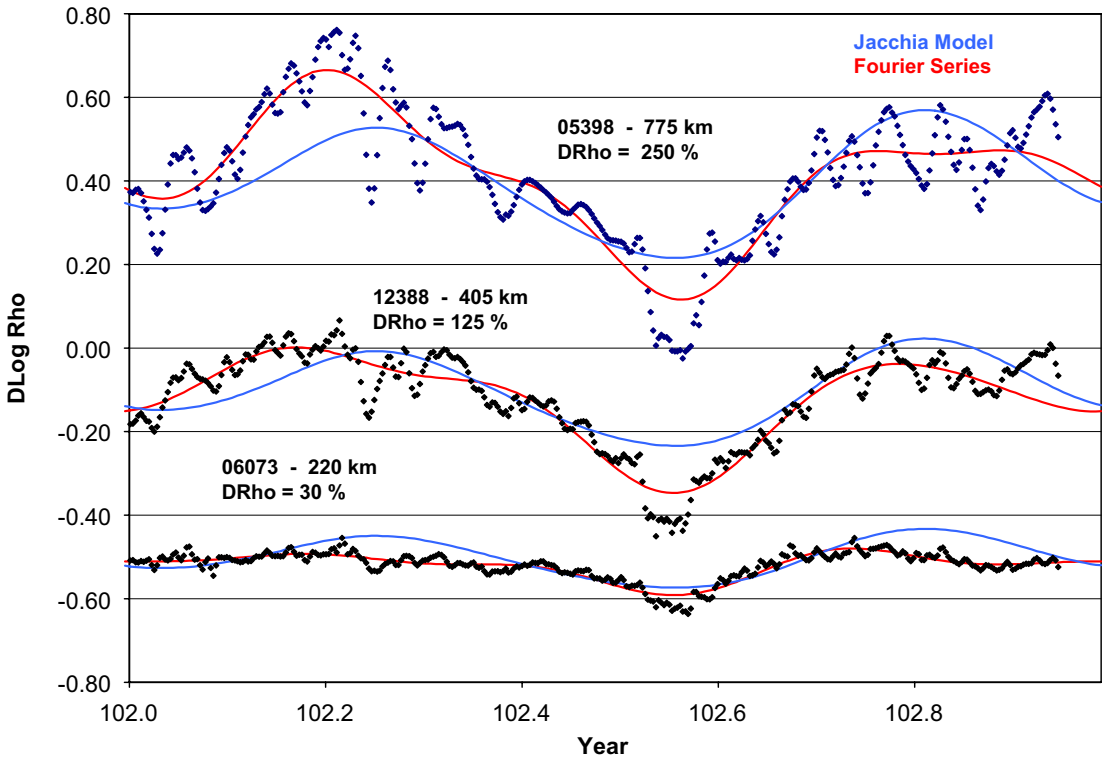

Fig. 4. Semiannual density variation for 2002 for selected satellites. Individual points are daily density difference values. Jacchia's model and individual satellite Fourier fit are also plotted. The top and bottom set of curves have been offset in Dlog Rho ($\Delta \log_{10} \rho$) by +0.5 and −0.5, respectively, for clarity.

It was previously determined (Bowman, 2004) that a Fourier series could accurately represent Jacchia's $G(t)$ equation structure and simplify the solution of the coefficients. It was determined that a 9 coefficient series, including frequencies up to 4 cycles per year, was sufficient to capture all the variability in $G(t)$ that had been previously observed.

It was also determined that a simplified quadratic polynomial equation in z could sufficiently capture Jacchia's $F(z)$ equation and not lose any fidelity in the observed $F(z)$ values.

The resulting equations used for modeling the observed yearly variations were

$$F(z) = B_1 + B_2 z + B_3 z^2 \ (z \text{ in km}), \tag{3}$$

$$G(t) = C_1 + C_2 \sin(\omega) + C_3 \cos(\omega) + C_4 \sin(2\omega) + C_5 \cos(2\omega) + C_6 \sin(3\omega) + C_7 \cos(3\omega) + C_8 \sin(4\omega) + C_9 \cos(4\omega), \tag{4}$$

where $\omega = 2\pi\vartheta$, $\vartheta = (t - 1.0)/365$, and $t =$ day of year.

4.2. Semiannual $F(z)$ height function

The amplitude, $F(z)$, of the semiannual variation was determined on a year-by-year and satellite-by-satellite basis. The smoothed density difference data were fit each year for each satellite using the 9-term Fourier series (Eq. (4)). The $F(z)$ value was then computed from each fit as the difference between the minimum and maximum values for the year.

Fig. 5 shows the results of 3 different years of data, along with the plot of Jacchia's $F(z)$ equation. For each year, the $F(z)$ values were fit with a quadratic polynomial in height. The smoothed curves shown in Fig. 5 represent the least-squares quadratic fit obtained for 3 different years. The $F(z)$ $\Delta\log_{10}\rho$ data for all satellites are very consistent within each year, producing a standard deviation of only 0.03. The most notable feature in Fig. 5 is the very large difference in maximum amplitude among the years displayed. The 2002 data show a maximum density variation of 250% near 800 km, while the 1993 data show only a 60% maximum variation. Jacchia's $F(z)$ function only gives a constant 130% maximum variation for all years.

To obtain a global fit, covering all years and all heights, all $F(z)$ values for all satellites and all years were fitted to obtain the $F(z)$ global function using the following equation:

$$F(z) = B_1 + B_2\bar{F}_{10} + B_3\bar{F}_{10}z + B_4\bar{F}_{10}z^2 + B_5\bar{F}_{10}^2 z + B_6\bar{F}_{10}^2 z^2, \tag{5}$$

where z is the (height (km)/1000) and $\bar{F}_{10}$ is the 81-day centered average of F_{10}. Since the $F(z)$ value for each year is defined as the difference between the yearly maximum and yearly minimum values this necessitates using a single $\bar{F}_{10}$ value to correspond

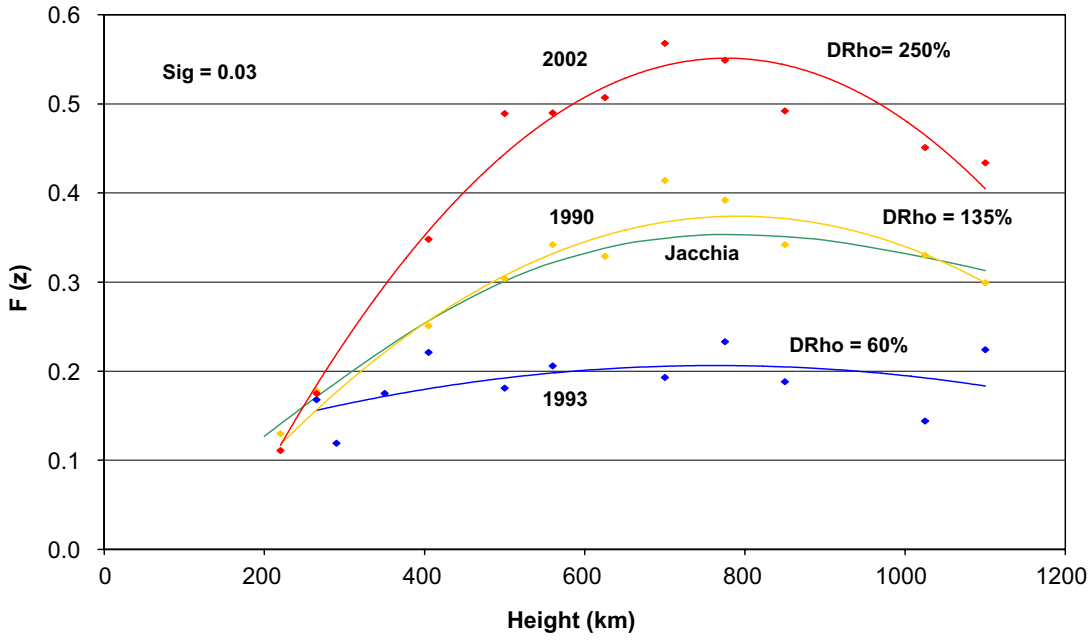

Fig. 5. The amplitude function $F(z)$ for 3 different years (1990, 1993, and 2002), with semiannual amplitudes plotted for each satellite for each year. The standard deviation, 'sig', of the fits is shown. The constant $F(z)$ function from Jacchia is also plotted.

to this yearly $F(z)$ value in solving for the coefficients in Eq. (5). The $\bar{F}_{10}$ value at each yearly observed semiannual minimum time of occurrence was selected for the coefficient determination. This will introduce an approximation into Eq. (5), which will be even more approximated from evaluating the $F(z)$ value on a daily basis using the current daily $\bar{F}_{10}$ value to compute the daily semiannual variation value. Table 2 shows Eq. (5) B global coefficients for $F(z)$ used in the JB2006 model.

Fig. 6 shows the observed yearly $F(z)$ values at 500 km and the fitted $F(z)$ global values at 500 km plotted as a function of year. Also shown are the average $\bar{F}_{10}$ values. The strong correlation of the yearly $F(z)$ values with $\bar{F}_{10}$ is readily apparent. Also apparent are the occasional large deviations in the observed values from the global model values. These deviations are mostly the result of large variations in the 27-day F_{10} flux occurring during the July semiannual minimum time.

Table 2
Eq. (5) coefficients for global $F(z)$ function

B coefficient	Term	Value
1	1	1.11613E−01
2	F	−1.59000E−03
3	$F \times Z$	1.26190E−02
4	$F \times Z^2$	−1.00064E−02
5	$F^2 \times Z$	−2.37509E−05
6	$F^2 \times Z^2$	2.60759E−05

$F = \bar{F}_{10}$ and $Z = z$ height function.

4.3. Semiannual $G(t)$ yearly periodic function

The $G(t)$ yearly function, as previously discussed, consists of a Fourier series with 9 coefficients. The 28-day smoothed density difference data for each satellite were fitted with the Fourier series for each year. The density difference data are the accurate observed daily density values minus the Jacchia values without Jacchia's semiannual variation. The $G(t)$ function was then obtained by normalizing to a value of 1 the difference between the minimum and maximum values for the year. The $F(z)$ value for each satellite by year was used for the normalization. Fig. 7 shows the results obtained for the year 1990 for the majority of the satellites. Note the tight consistency of the curves for all heights, covering over 800 km in altitude. A yearly $G(t)$ function was then fit using the data for all the satellites for each year. Fig. 7 also shows the yearly $G(t)$ equation values, with a standard deviation of 0.11 in $\Delta \log_{10} \rho$. A small sigma was obtained for every year's fit, especially during solar maximum years. Fig. 8 shows the yearly $G(t)$ fits for 1999

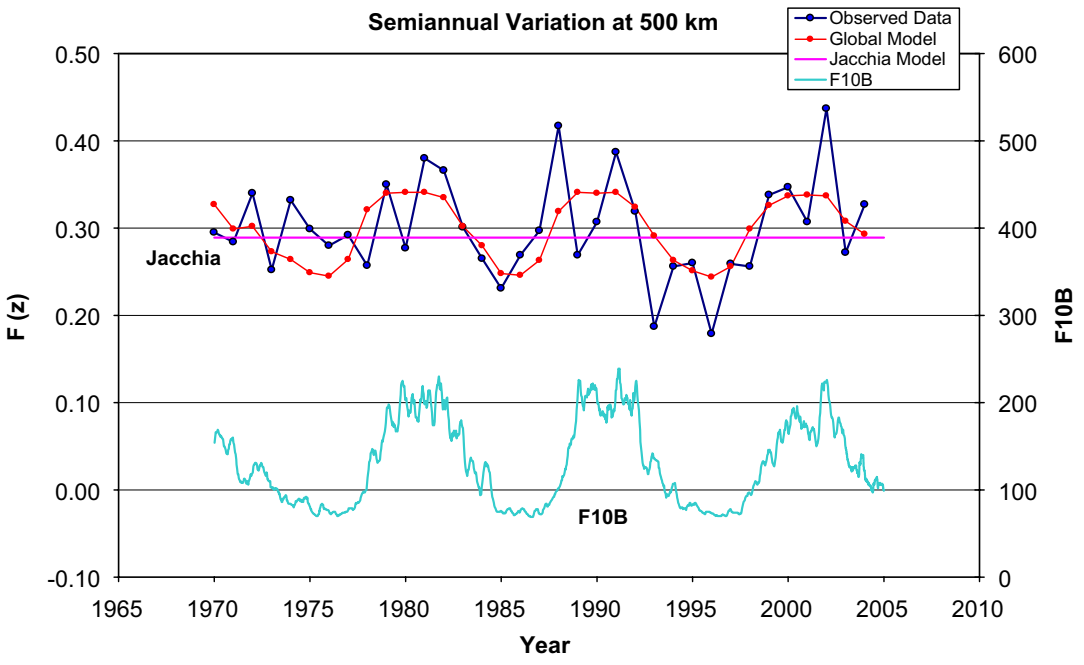

Fig. 6. The observed $F(z)$ value at 500 km height for each year plotted by year. Also shown are the computed global $F(z)$ values. The $\bar{F}_{10}$ average, F10B, is displayed, along with Jacchia's constant 500 km amplitude value.

through 2001. It is readily apparent that the series changes dramatically from year to year. During solar maximum the July minimum date can vary by as much as 80 days. The variability is especially large for defining the time of the July minimum during solar maximum, while the solar minimum July minimum times are much more consistent from year to year.

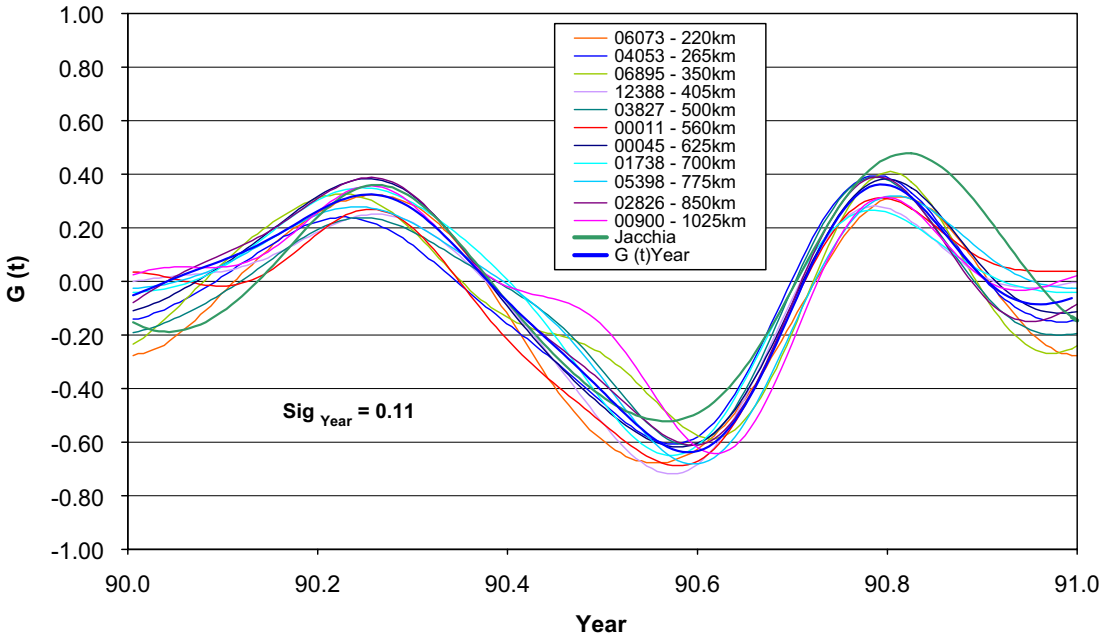

Fig. 7. The individual satellite $G(t)$ fits are plotted for 1990. The Jacchia model and yearly fit equation values are also shown. The standard deviation, 'Sig_{Year}', for the year $G(t)$ equation values are displayed.

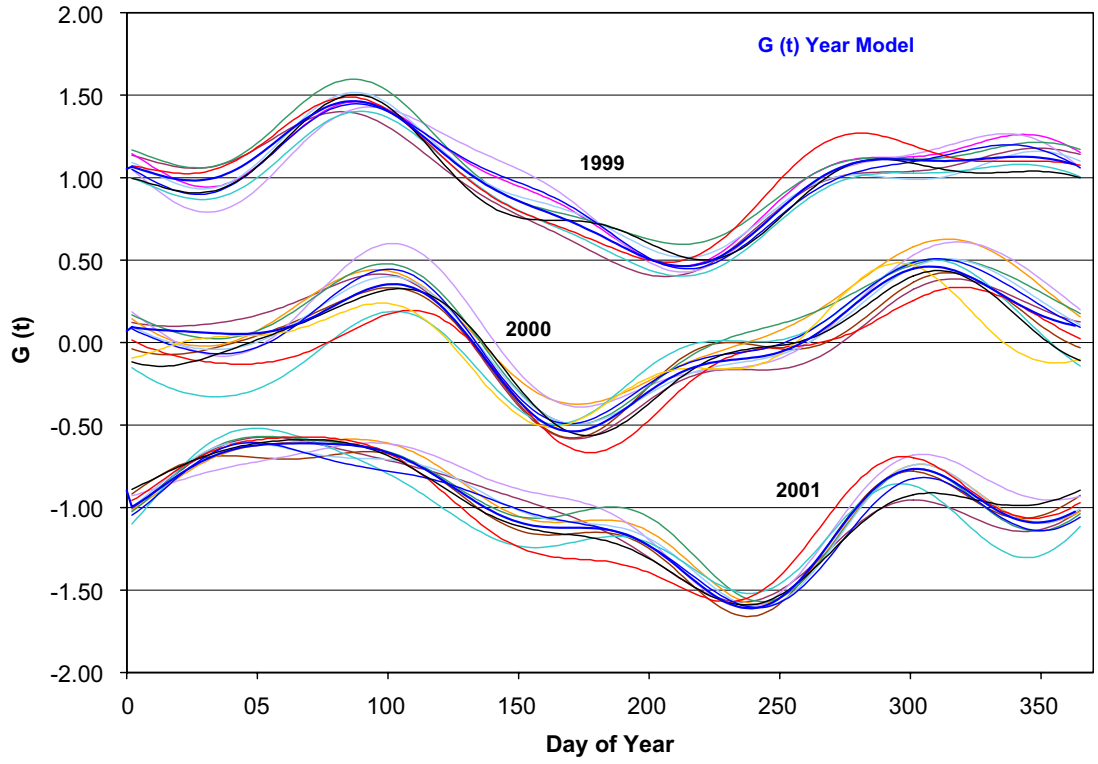

Fig. 8. The individual satellite fits for 3 different years are shown. The year $G(t)$ equation values are highlighted. Each set of curves for 1999 and 2001 has been offset by $+1.00$ and -1.00, respectively, in $G(t)$ for clarity.

4.4. Semiannual $G(t)$ global function

A global $G(t)$ function was obtained using all satellite data for all years. Since the yearly $G(t)$ functions demonstrated a dependence on solar activity, it was decided to expand the series as a function of the average $\bar{F}_{10}$. The following equation was finally adopted for the global $G(t)$ function:

$$\begin{aligned} G(t) = {} & C_1 + C_2 \sin(\omega) + C_3 \cos(\omega) + C_4 \sin(2\omega) \\ & + C_5 \cos(2\omega) + C_6 \sin(3\omega) + C_7 \cos(3\omega) \\ & + C_8 \sin(4\omega) + C_9 \cos(4\omega) \\ & + \bar{F}_{10}\{C_{10} + C_{11} \sin(\omega) + C_{12} \cos(\omega) \\ & + C_{13} \sin(2\omega) + C_{14} \cos(2\omega) + C_{15} \sin(3\omega) \\ & + C_{16} \cos(3\omega) + C_{17} \sin(4\omega) + C_{18} \cos(4\omega)\} \\ & + \bar{F}_{10}^2\{C_{19} + C_{20} \sin(\omega) + C_{21} \cos(\omega) \\ & + C_{22} \sin(2\omega) + C_{23} \cos(2\omega)\}, \end{aligned} \quad (6)$$

where $\omega = 2\pi\vartheta$, $\vartheta = (t - 1.0)/365$, and $t =$ day of year.

Table 3 lists the least-squares fitted values for the C_i coefficients in Eq. (6) that are used in the JB2006 model.

Fig. 9 is a plot of the global $G(t)$ Eq. (6) as fitted with all the satellite data. Jacchia's equation for $G(t)$ is also shown. It is interesting to note that the solar minimum and solar maximum plots are significantly different except near the October maximum, which appears to have only a slight phase shift among the different curves. The April maximum variation is much larger in amplitude, though not in phase. Jacchia's function overestimates the October maximum for all solar activity, and only correctly estimates the April maximum during average solar activity. The curves once again demonstrate the need for solar activity to be included in the semiannual $G(t)$ function.

The resulting new semiannual equation for $\Delta_{SA}\log_{10}\rho$ used in the JB2006 model is obtained using $F(z)$ and $G(t)$ from Eqs. (5) and (6) in the standard semiannual Eq. (2).

5. Diurnal density correction

Daily temperature corrections (Bowman et al., 2004), dT_c, to the Jacchia 1970 atmospheric model were obtained on 79 calibration satellites for the period 1994 through 2003, and 35 calibration satellites for the solar maximum period 1989 through 1990. All the "calibration" satellites have moderate to high eccentricity orbits, with perigee heights ranging from 150 to 500 km. This means that the daily dT_c correction value obtained for a satellite represents the temperature correction needed for a specific local solar time, latitude, and height corresponding to the perigee location.

Corrections to the diurnal (local solar time) and latitude equations were then obtained in the following manner. The dT_c values on all the calibration satellites were least-squares fit daily as a function of height. These daily fits represented the global dT_c correction on a day-by-day basis. The daily fit values of dT_c were then removed from the original dT_c temperature corrections obtained for each satellite. The resulting ΔT_c corrections could then be attributed to model errors in local solar time and latitude. The original approach to correct the observed model errors was to obtain, using the new ΔT_c values, new coefficients to Jacchia's original diurnal equations. However, this proved unfruitful because of the complexity of the

Table 3
C coefficient values for Eq. (6), where $F = \bar{F}_{10}$

C coeffcient	Term	Value	C coefficient	Term	Value
1	1	−0.833646D+00	13	$F \times \sin 2\omega$	0.206763D−02
2	$\sin\omega$	−0.265450D+00	14	$F \times \cos 2\omega$	−0.142888D−02
3	$\cos\omega$	0.467603D+00	15	$F \times \sin 3\omega$	−0.867124D−05
4	$\sin 2\omega$	−0.299906D+00	16	$F \times \cos 3\omega$	0.189032D−04
5	$\cos 2\omega$	−0.105451D+00	17	$F \times \sin 4\omega$	0.156988D−03
6	$\sin 3\omega$	−0.165537D−01	18	$F \times \cos 4\omega$	0.491286D−03
7	$\cos 3\omega$	−0.380037D−01	19	F^2	−0.391484D−04
8	$\sin 4\omega$	−0.150991D−01	20	$F^2 \times \sin\omega$	−0.126854D−04
9	$\cos 4\omega$	−0.541280D−01	21	$F^2 \times \cos\omega$	0.134078D−04
10	F	0.119554D−01	22	$F^2 \times \sin 2\omega$	−0.614176D−05
11	$F \times \sin\omega$	0.437544D−02	23	$F^2 \times \cos 2\omega$	0.343423D−05
12	$F \times \cos(\omega)$	−0.369016D−02			

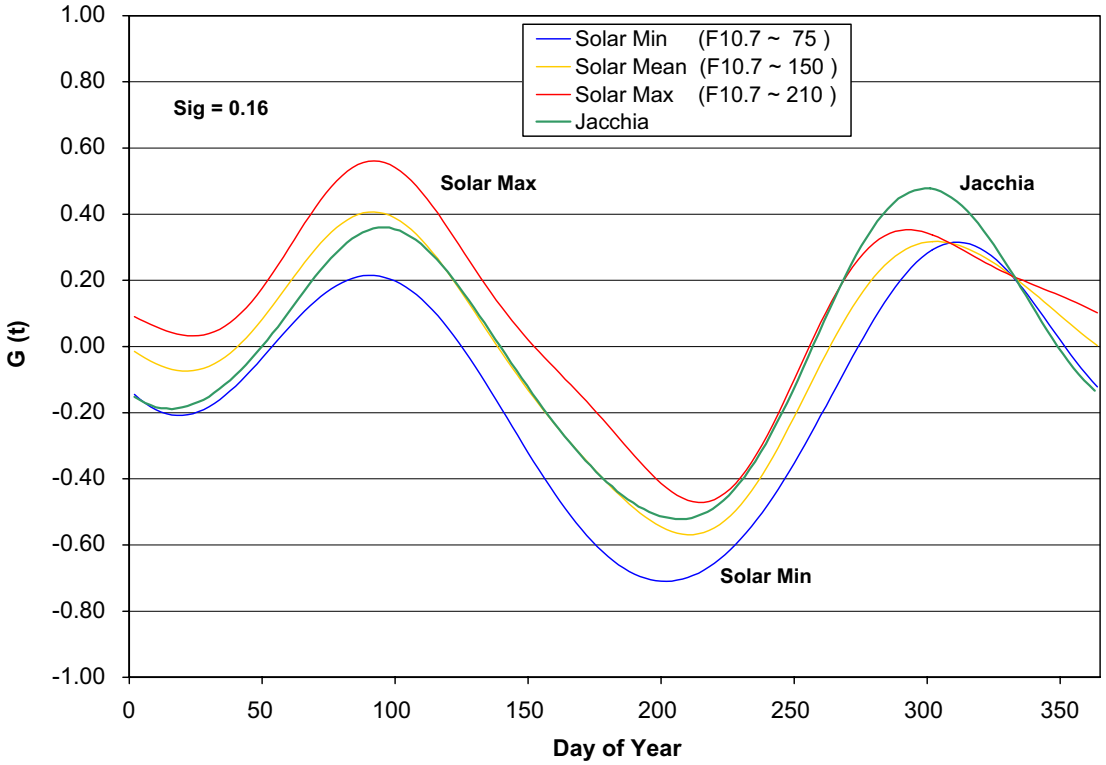

Fig. 9. The $G(t)$ curves for different solar activities as computed from the $G(t)$ global equation are shown. The standard deviation, 'Sig', of the global fit is displayed.

errors, so a polynomial approach was adopted. Since the observed errors showed variations as a function of local solar time, latitude, height, and F_{10}, the objective was to obtain polynomial fits with the least number of trigonometry functions to facilitate computer computation time. These daily ΔT_c values were all lumped together, and equations were least-squares fit as a function of local solar time, latitude, height, and solar flux. Fig. 10 shows the ΔT_c values at 200–300 km altitude along with the fitted equation as a function of local solar time. The ΔT_c values are for solar minimum conditions. Fig. 11 shows the ΔT_c values with the fitted equation for solar maximum conditions at an altitude of 400–500 km. Finally, Fig. 12 shows the fitted equations in ΔT_x for a range of altitudes below 200 km for moderate solar conditions. The correction in T_x (Jacchia, 1971), the inflection point temperature, was used for heights below 200 km because it better represented density variations than T_c for these very low altitudes. As can be seen in the figures the ΔT_c correction equations vary significantly with respect to local solar time, height, and solar flux. The resulting ΔT_c equations are divided into heights above 250 km (Eq. (7)) and between 200 and 250 km (Eq. (8)). Below 200 km a ΔT_x correction (Eq. (9)) was obtained. The intermediate altitude Eq. (8) was obtained from spline fitting Eq. (7) with the boundary conditions in ΔT_c obtained from Eq. (9), where the boundary value and slope of Eq. (8) agree with the values of Eq. (7) and the ΔT_c values computed from Eq. (9) at the respective boundary altitudes. Table 4 lists all the coefficients values for these three equations.

Finally, either the ΔT_c or the ΔT_x values computed from Eq. (7), (8), or (9) are added to the T_c or T_x values (from Jacchia, 1970) in the JB2006 model to obtain the T_c and T_x values used for the density computations.

F	$(F_{10}-100)/100$
θ	(local solar time(h))/24
φ	cos (latitude)
z	height (km)

For 700 km $> z \geqslant$ 250 km: $H = z/100$,

$$\begin{aligned}\Delta T_c = {} & B_1 + F(B_2 + B_3\theta + B_4\theta^2 + B_5\theta^3 + B_6\theta^4 + B_7\theta^5) \\ & + \phi(B_8\theta + B_9\theta^2 + B_{10}\theta^3 + B_{11}\theta^4 + B_{12}\theta^5) \\ & + \phi H(B_{13} + B_{14}\theta + B_{15}\theta^2 + B_{16}\theta^3 \\ & + B_{17}\theta^4 + B_{18}\theta^5) + B_{19}\phi. \end{aligned} \quad (7)$$

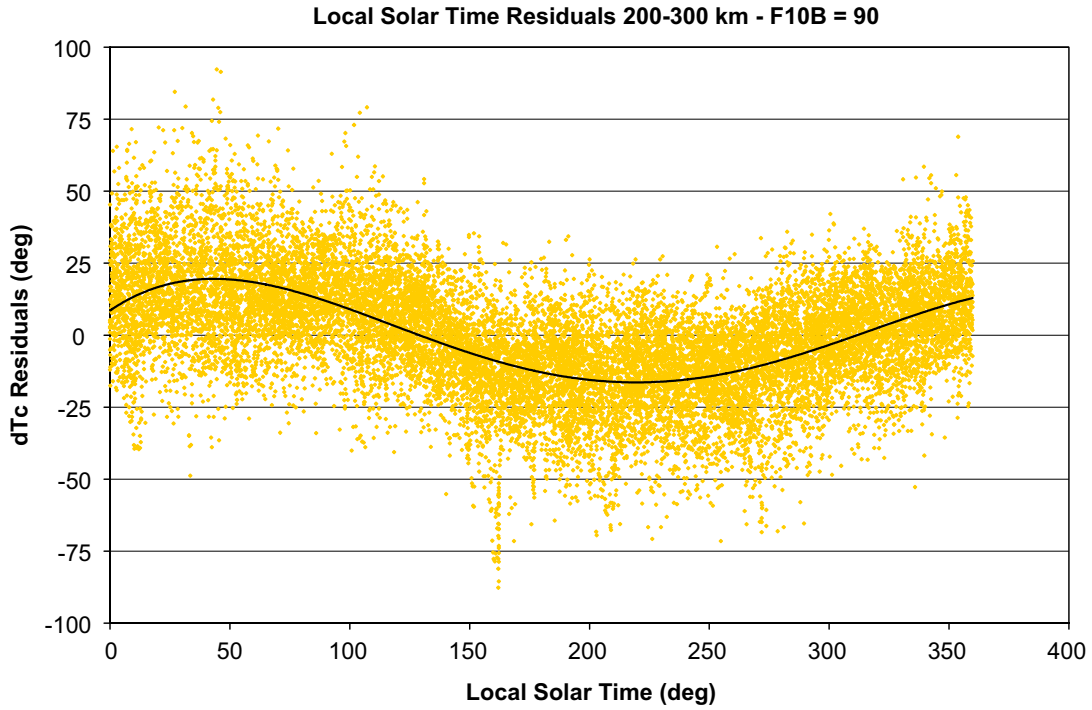

Fig. 10. ΔT_c values for solar minimum conditions as a function of local solar time.

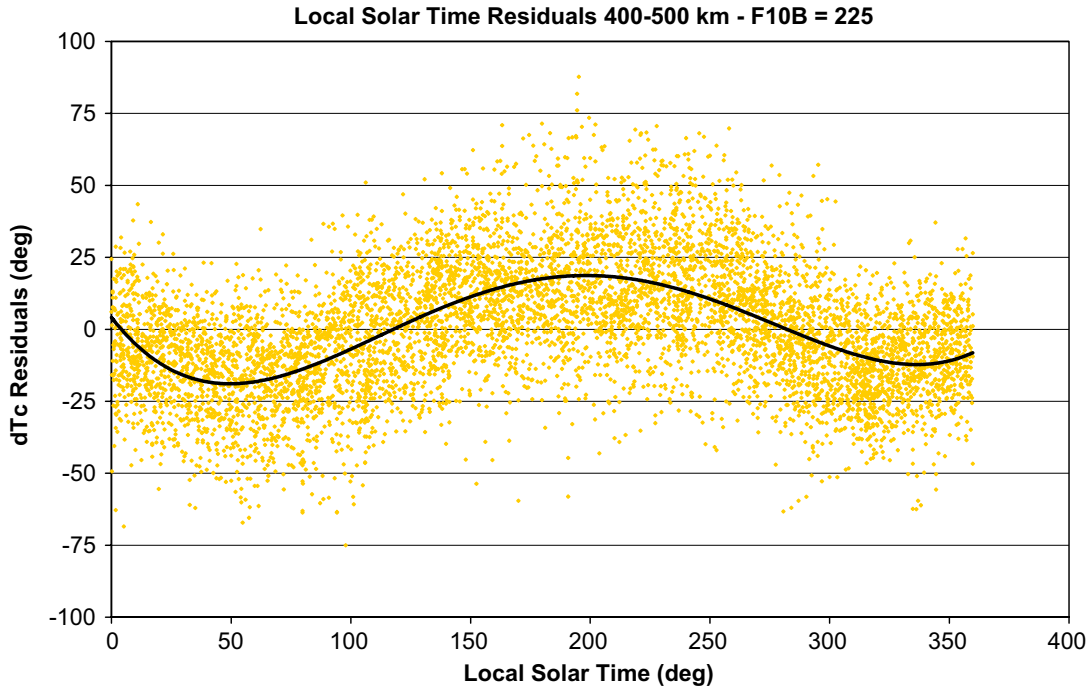

Fig. 11. ΔT_c values for solar maximum conditions as a function of local solar time.

For $250\,\text{km} \geqslant z \geqslant 200$: $H = (z-200)/50$,

$$\begin{aligned}\Delta T_c = {} & HC_1 + HF(C_2 + C_3\theta + C_4\theta^2 + C_5\theta^3 \\ & + C_6\theta^4 + C_7\theta^5) + H\phi(C_8\theta + C_9\theta^2 + C_{10}\theta^3 + C_{11}\theta^4 \\ & + C_{12}\theta^5 + C_{13} + C_{14}F + C_{15}F\theta + C_{16}F\theta^2) \\ & + C_{17} + \phi(C_{18}\theta + C_{19}\theta^2 + C_{20}\theta^3 + C_{21}F \\ & + C_{22}F\theta + C_{23}F\theta^2). \end{aligned} \quad (8)$$

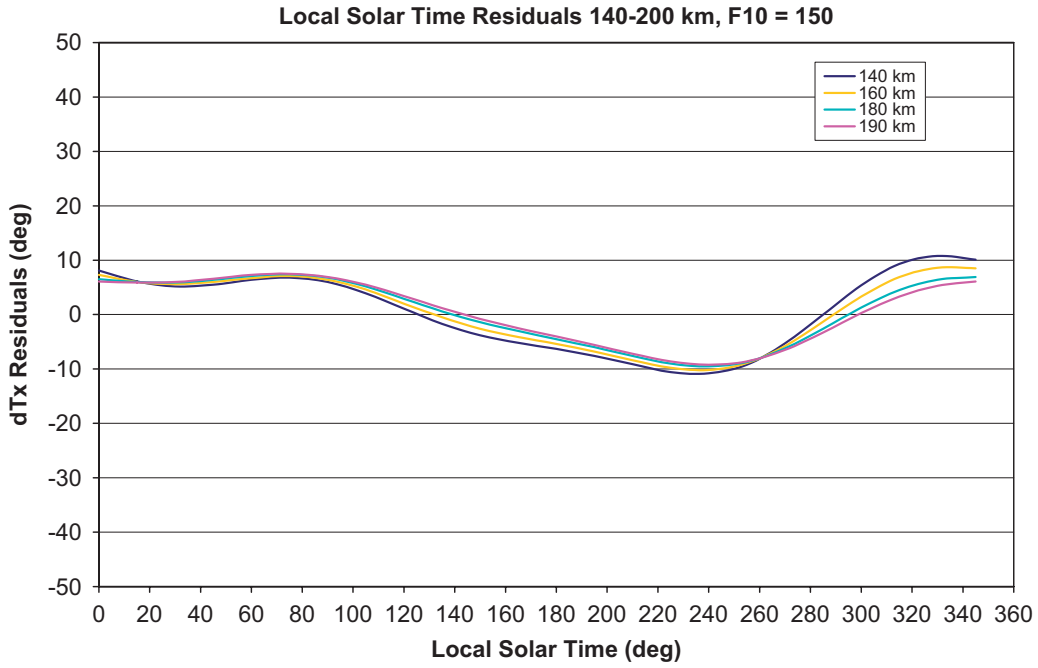

Fig. 12. ΔT_x values for solar moderate conditions as a function of local solar time and altitude.

Table 4
Coefficient values for Eqs. (7), (8), and (9)

Coefficient	*B* value	*C* value	*D* value
1	−0.457512297D + 01	−0.155986211D + 02	0.828727388D + 00
2	−0.512114909D + 01	−0.512114909D + 01	0.124730376D + 02
3	−0.693003609D + 02	−0.693003609D + 02	−0.318077422D + 03
4	0.203716701D + 03	0.203716701D + 03	0.645905237D + 03
5	0.703316291D + 03	0.703316291D + 03	−0.322577619D + 03
6	−0.194349234D + 04	−0.194349234D + 04	0.709584573D + 01
7	0.110651308D + 04	0.110651308D + 04	0.126347673D + 02
8	−0.174378996D + 03	−0.220835117D + 03	−0.744574342D + 02
9	0.188594601D + 04	0.143256989D + 04	0.511241177D + 02
10	−0.709371517D + 04	−0.318481844D + 04	−0.354195845D + 01
11	0.922454523D + 04	0.328981513D + 04	0.225275051D + 02
12	−0.384508073D + 04	−0.135332119D + 04	−0.223771015D + 02
13	−0.645841789D + 01	0.199956489D + 02	
14	0.409703319D + 02	−0.127093998D + 02	
15	−0.482006560D + 03	0.212825156D + 02	
16	0.181870931D + 04	−0.275555432D + 01	
17	−0.237389204D + 04	0.110234982D + 02	
18	0.996703815D + 03	0.148881951D + 03	
19	0.361416936D + 02	−0.751640284D + 03	
20		0.637876542D + 03	
21		0.127093998D + 02	
22		−0.212825156D + 02	
23		0.275555432D + 01	

For 200 km $\geqslant z \geqslant$ 140: $H = z/100$,

$$\Delta T_x = D_1 + (D_2\theta + D_3\theta^2 + D_4\theta^3 + D_5\theta^4) + H(D_6 + D_7\theta + D_8\theta^2 + D_9\theta^3) + F(D_{10} + D_{11}\theta + D_{12}\theta^2). \quad (9)$$

6. High-altitude density correction

All atmospheric models developed to date have only been able to incorporate small amounts of neutral density values above 1000 km due to lack of

data at these higher altitudes. The models developed by Jacchia (1970, 1971 and 1977) only used a few satellites to correlate long-term density variations with the 11-year variation of the $\bar{F}_{10}$ index, and those satellites were all below 800 km altitude. Later work by Hedin (1983, 1987, 1991) in developing the MSIS models still used only density data below 1000 km. Only a handful of density analyses have been done for satellites in the 1500–4000 km height range. A number of papers were published in the 1970s based on analyses of the orbital decay of the Pageos 1 and Dash-2 balloons. Prior (1971) found hydrogen concentrations about three times that of the US Standard 1966 Atmosphere Supplement (COESA, 1966) for both Pageos and Dash-2 during 1967 when they were at approximately 3500 km altitude. Rousseau (1973) analyzed Dash-2 data in the height range of 1500–3000 km and found that the Jacchia 70 model underestimated the density values by about a factor of 3. Slowey (1974) reduced Dash-2 data for selected time spans between 1964 and 1971, and found that the Jacchia 70 model again underestimated the density by about a factor of 3. From the previous analyses it appeared that the Jacchia 70 model underestimated the densities at 1500–3500 km by up to a factor of 3, which prompted a more complete analysis of this underestimated high-altitude variation.

The above-mentioned analyses for the height range of 1500–4000 km covered only a short time span relative to the solar 11-year sunspot cycle, and thus no correlation was obtained between density variations and the $\bar{F}_{10}$ solar index. The current JB2006 model uses a recent analysis (Bowman, 2001) of over 30 years of density data, in the height range of 1500–4000 km obtained from 25 satellite orbits, to formulate density variations with respect to altitude and the $\bar{F}_{10}$ index.

6.1. High-altitude density analysis

The analysis method was described previously (Bowman, 2002) from the long-term orbit perturbation analysis of West Ford needles' orbits. A semi-analytical integrator was developed using the perturbations in the semi-major axis from atmospheric drag, solar radiation pressure, and earth albedo. The drag equations consisted of orbit-averaged perturbation equations derived by King-Hele (1964). The solar radiation pressure equations were orbit-averaged equations in the semi-major axis developed by Koskela (1962). The earth albedo model consisted of orbit-averaged equations developed by Anselmo et al. (1983), where albedo perturbations on the semi-major axis accounted for the albedo differences of the northern and southern hemispheres.

The atmospheric drag equations required modification for the variation of the drag coefficient. For a circular satellite below 600 km height, the C_D value remains almost constant at 2.2 throughout the 11-year solar cycle. However, C_D is a function of the mass and velocity of the atmospheric constituents, which means that it will increase with altitude as the abundance of the lighter elements increases with altitude. As the height increases, the lighter atomic and molecular species become predominant, depending upon the level of solar activity present. At 3500 km the C_D value can be higher than 4.0, where atomic hydrogen is the dominant species during solar minimum. Fig. 13 shows the log densities of the different high-altitude species as a function of solar activity. During high solar activity, atomic oxygen is dominant at altitudes from 500 up to 1200 km, while during solar minimum conditions it loses dominance just above 500 km. During solar minimum the lightest element hydrogen becomes dominant above 800 km, while during solar maximum it does not start showing an effective presence until altitudes over 4000 km have been reached. Therefore, the C_D value changes greatly depending upon altitude and solar conditions.

For analyzing the data a non-linear least-squares program was developed to fit the NORAD mean semi-major axis (a) values. For each satellite included in the analysis the semi-major axis was integrated over a data span between 20 and 35 years, depending upon data availability. The perturbations from the orbit-averaged equations were integrated over the span with a 2-day step size. The semi-major axis was used as the element of interest, since there are no long periodic or secular perturbations in a from any gravitational effects for these orbits of interest. NORAD mean elements were available every 3–10 days for the satellites for up to 35-year time spans. During the integration the other predicted orbital elements were constrained to the values of the real mean elements obtained from the NORAD element sets. This method avoids non-linear variations in a, and allows good convergence in the solution coefficients. The long-term solution parameters included density correction factors for hydrogen and helium, a direct solar radiation pressure coefficient, the initial semi-major axis

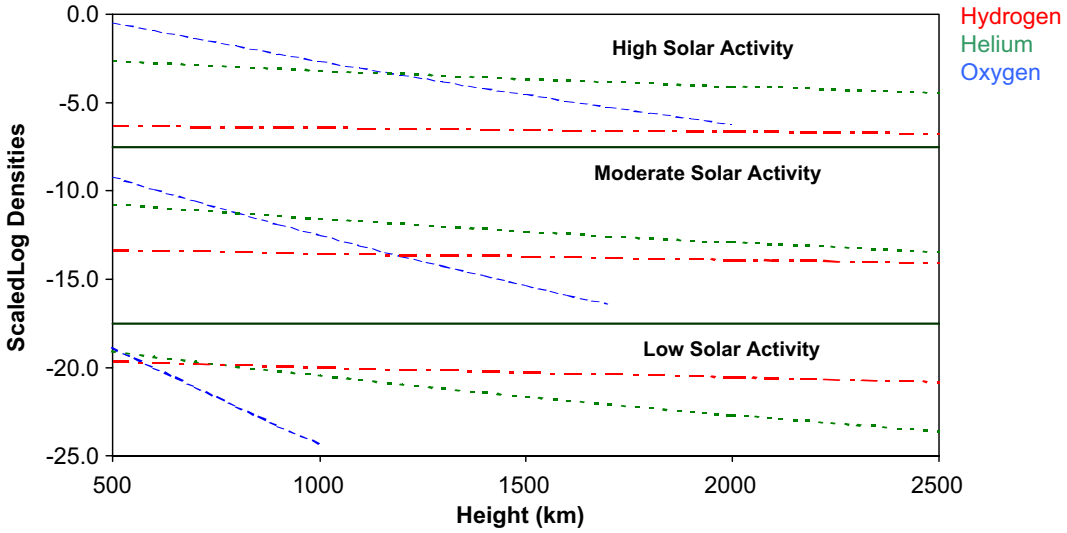

Fig. 13. Species abundances as a function of altitude and solar conditions. The three regions above are separately scaled in log densities for clarity.

value, and several long-term albedo coefficients (Bowman, 2002). The drag coefficient C_D was modeled to account for the dominance of different atomic and molecular species. Each fit consisted of using 500–1000 sets of orbit elements. The density factors obtained for hydrogen and helium represent 20–35 year averages of density variations at altitudes above 1500 km. The density factors are multiplication factors of the CIRA72 species densities before all the species densities are combined into the model density value used in the drag equations. The CIRA72 model atmosphere was selected for the analysis because it integrates the diffusion equations to any altitude as opposed to using predefined lookup tables that stop at 2500 km altitude. The previous paper (Bowman, 2002) lists the fit results for 20 West Ford needle clusters.

The long-term (20–35 year) best-fit solution for each satellite contains the solar radiation pressure and albedo coefficients for the satellite. The previous analysis demonstrated that the satellite area-to-mass (A/M) ratio could be determined within 15% accuracy using each satellite solution's long-term solar radiation pressure coefficient. Once the A/M ratio was determined, short-term density factors could be obtained by holding the long-term solar radiation pressure and albedo coefficients constant, and fitting only the initial a and one density factor for each short interval selected. The resulting density factor represents a 1–2 year average compared with the CIRA72 density values. Fits of less than 1 year showed too much variability in the drag coefficients, which is typical of least-squares orbit determinations when coefficient observability is a problem. Thus, the short-term fit spans were limited to 1–2 year intervals based on drag coefficient observability.

Density factors were obtained for 25 satellites spanning a period of over 30 years. Eighteen West Ford needle clusters were used in the height range of 1450–3600 km. All the needle clusters had large A/M ratios greater than 0.75 m^2/kg. Five pieces of Delta 1 rocket body debris were used for density variations in the height range of 1600–1750 km. The A/M ratios of these pieces were all greater than 0.10 m^2/kg, which was sufficient to determine density variations at these lower altitudes. Finally, two balloon satellites, Pageos-1 and Dash-2, were included in the analysis.

Following determination of the 1–2 year average density factors for each satellite, the data were plotted with respect to time and the 81-day average $\bar{F}_{10}$ solar index. Fig. 14 shows an example of the data obtained for the needle cluster 02530 over the 30-year period of analysis for this satellite. The factors can be separated into periods when hydrogen was dominant ($\rho_{He}/\rho_H < 0.3$), when helium was dominant ($\rho_{He}/\rho_H > 3$), and when an approximately even mixture of hydrogen and helium occurred. The CIRA72 model was used to determine the concentration of each species. Satellite 02530 remained in the height range of 3000–3600 km during the entire 30-year span. Fig. 14 shows that hydrogen was dominant during periods of low solar activity ($\bar{F}_{10} < 90$), while helium was dominant during periods of high solar activity ($\bar{F}_{10} > 150$).

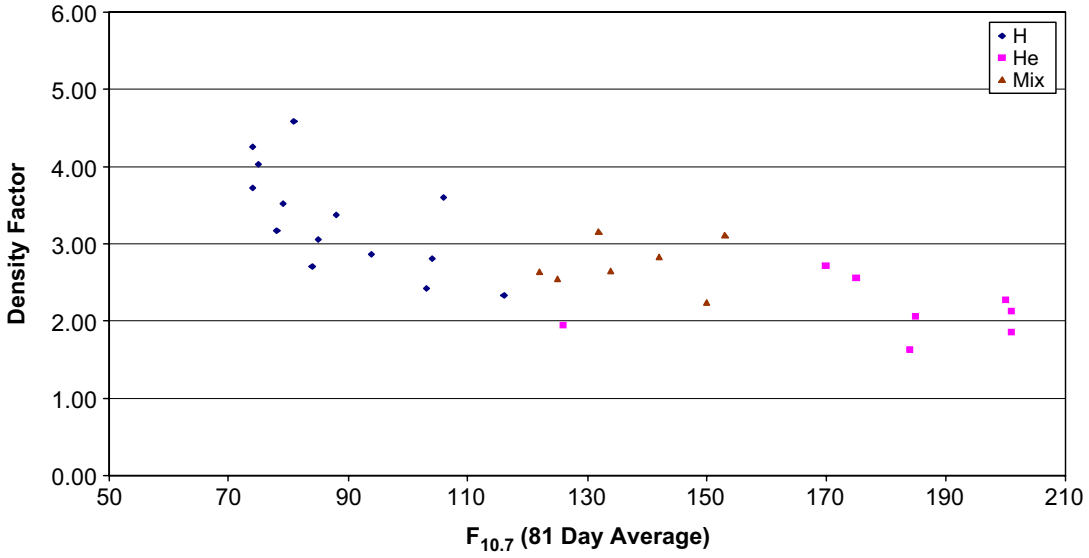

Fig. 14. Density factors obtained for satellite 02530 from 1970 through 2000 as a function of $\bar{F}_{10}$, with the dominant species shown for the different solar conditions.

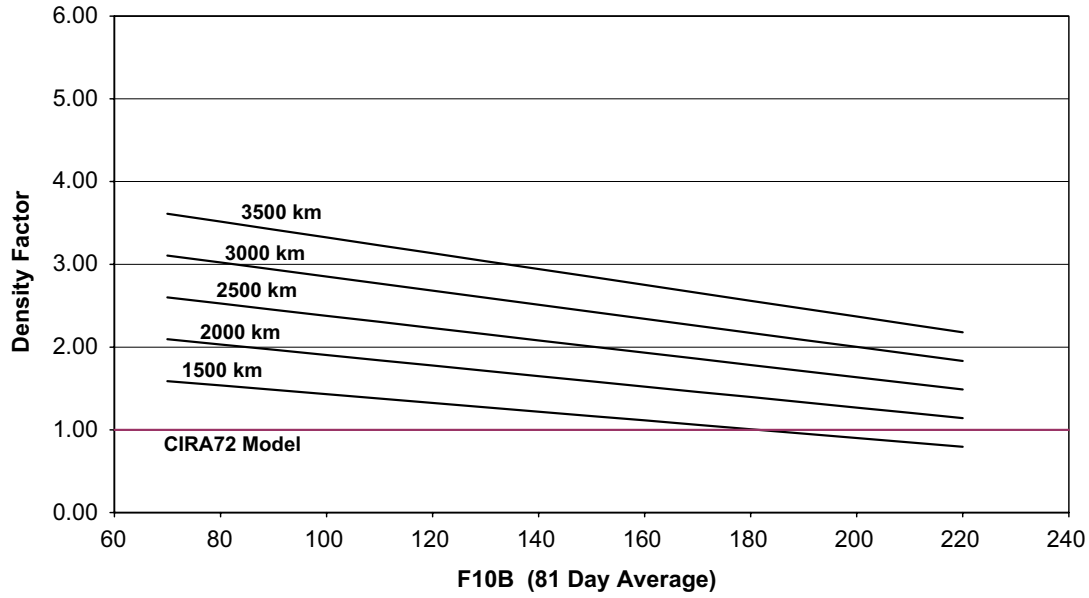

Fig. 15. Density factors for the CIRA72 (Jacchia 71) model plotted as a function of altitude and $\bar{F}_{10}$ for altitudes from 1000 to 3500 km.

Approximately 500 density factors were obtained from data from all 25 satellites covering more than 30 years of time. The density factors were then fit as a function of height and $\bar{F}_{10}$.

6.2. High-altitude density equations

The new JB2006 equation plots are shown in Fig. 15 as a function of height and $\bar{F}_{10}$ values. The least-squares model obtained from fitting the factor data for $z > 1500$ km is

$$F_\rho = C_1 + C_2\bar{F}_{10} + C_3 z + C_4 z\bar{F}_{10}, \quad (10)$$

where z is the height (km) and $\bar{F}_{10}$ the 81-day F_{10} average (Table 5).

Between 1000 km (factor = 1.0) and 1500 km the factor equation was obtained as a spline fit (factor value and slope equal at boundary values of 1000 and 1500 km).

For 1500 km $> z >$ 1000 km the spline-fit equation is

$F\rho(H)$ = density factor, $H = (z-1000)/500$,

F_{1500} = density factor at 1500 km,

$\partial F_{1500}/\partial z = 500(C_3 + C_4\bar{F}_{10})$, partial of density factor at 1500 km,

$$F_\rho(H) = 1 + \left\{3F_{1500} - 500\frac{\partial F_{1500}}{\partial z} - 3\right\}H^2 + \left\{500\frac{\partial F_{1500}}{\partial z} - 2F_{1500} + 2\right\}H^3, \quad (11)$$

where F_ρ is the density factor applied to the JB2006 high-altitude density computations.

The plots in Fig. 15 agree very well with other authors' previous results mentioned earlier, with the Jacchia models underestimating the densities in the 1500–3500 km altitude range by up to a factor of 3.5, depending upon solar conditions.

Table 5
Coefficient values for equation (10), where $F = \bar{F}_{10}$

C Coefficient	Term	Value
1	1	2.200E−01
2	F	−2.000E−03
3	Z	1.150E−03
4	$F \times z$	−2.110E−06

7. Model density errors

The new equations described above were incorporated into the JB2006 model, and differential orbit corrections were obtained on different satellites using this new model. Fig. 16 shows a plot of delta ballistic coefficient values (corrections to the 30-year average value) for one of the satellites during 2001. A value of 0% indicates that the atmospheric model correctly modeled the density during the orbit fit. The JB2006 curve uses the full JB2006 model, the Jacchia 70 curve uses the unmodified Jacchia 70 model, and the intermediate curve uses the JB2006 model but with the original Jacchia semiannual equations in place of the new JB2006 semiannual equations. The delta B values can be attributed strictly to density variations since this satellite is a sphere at a near constant perigee height of 400 km. The standard deviation has decreased from approximately 17% for the Jacchia model to just under 10% using the complete new JB2006 model. The intermediate curve shows that half of this decrease is due to the new semiannual equations. Additional orbit corrections showed that the new diurnal and latitudinal corrections accounted for approximately 0.5% reduction in the standard deviation. Therefore, the remaining

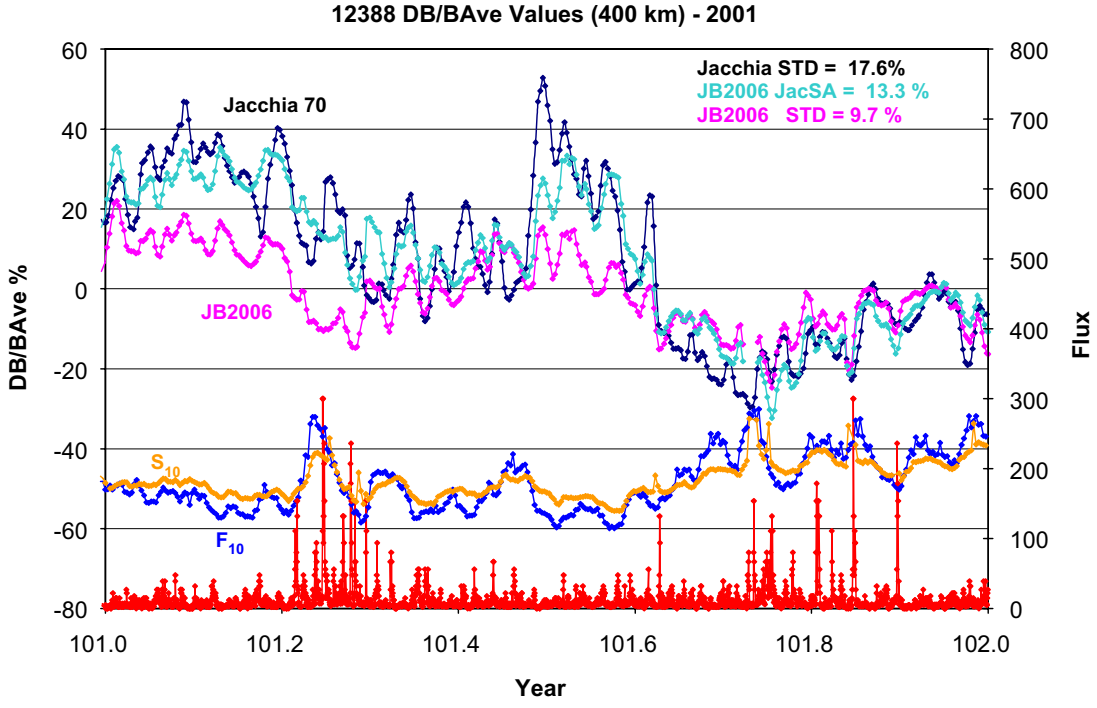

Fig. 16. Ballistic coefficient variations for satellite 12388 during 2001 from orbit determinations using Jacchia 70 and JB2006 atmospheric density models. The JB2006 JacSA curve is based on the new JB2006 model but with the J70 semiannual equations. The solar indices F_{10} and S_{10} along with the geomagnetic index a_p are also shown.

(almost half of the) decrease in the standard deviation can be attributed to using the new T_c equation with the new solar indices.

Several different atmospheric models were then used for comparison (Marcos et al., 2006) with the JB2006 model. The NASA Marshall Engineering Thermosphere (MET) model (Owens and Vaughan, 2004) was developed by the NASA Marshall Space Flight Center. The model is essentially J70, but with a 162-day averaged solar flux compared with the 81-day average of J70. It provides total mass density, temperature, and composition, and is used operationally for satellite lifetime estimates, orbit insertion, orbit determination and tracking, attitude dynamics, and reentry prediction. The drag temperature model (DTM) combined satellite drag, accelerometer, and satellite composition and temperature data to construct a three-dimensional thermospheric model (Barlier et al., 1978; Berger et al., 1998) of temperature, density, and composition based on diffusive equilibrium. An iterative procedure was used to obtain representation of the three major constituents N_2, O, and He in terms of spherical harmonics at 120 km altitude. Using a thermopause temperature model and an analytical temperature profile, concentrations for the major atmospheric constituents at a given altitude are computed as a function of solar and geophysical parameters. The current version of DTM (Bruinsma et al., 2003) has temperature and gradient at 120 km in agreement with ISR and satellite-borne interferometer data and AE data, and capability to use the MgII index in place of F_{10}. Our version of the model did not have this provision. Therefore, the model was eventuated using F_{10}.

The mass spectrometer and incoherent scatter (MSIS) series of models (Hedin 1977, 1983, 1987, 1991), developed between 1977 and 1990, are used extensively by the scientific community for their superior description of neutral composition. The models utilized atmospheric composition data from instrumented satellites and temperatures from ground-based radars. The initial MSIS 1977 model (Hedin et al., 1977) was based on the Jacchia temperature profile framework, but the density at 120 km varied with local time and other geophysical parameters to fit the measurements. Exospheric temperature and density variations were represented by spherical harmonics resulting in requiring fewer parameters for a given level of accuracy. Subsequent versions of the model include the longitude variations, a refined geomagnetic storm effect, improved high latitude, high solar flux data, and a boundary lowered to sea level. The NRLMSISE-00 (Picone et al., 2002) model of atmospheric composition, temperature, and total mass density from ground to exobase includes the following: (1) drag data based on orbit determination; (2) more recent accelerometer data sets; (3) new temperature data derived from Millstone Hill and Arecibo incoherent scatter radar observations; and (4) observations of (O_2) by the Solar Maximum Mission (SMM), based on solar UV occultation. A new species, "anomalous oxygen," primarily for drag estimation, allows for appreciable O^+ and hot atomic oxygen contributions to the total mass density at high altitudes.

Our primary objective was to evaluate density model performance in the 200–1100 km altitude region where satellite drag is the dominant source of tracking errors. We have an extensive representative set of data capable of evaluating models in the region of maximum importance, with densities from 37 satellites for the period from 1997 through 2004. The data were derived using the method of Bowman (2004) to obtain densities with 1-day temporal resolution for the first time from satellite tracking observations. The density errors are estimated to be less than 5%. Approximately 75,000 daily density values were obtained for the period 1997–2004 throughout the altitude region from about 200 to 1100 km.

The scope of the current database allows an unambiguous determination of model errors as a function of altitude. These errors for the JB2006, J70, NRLMSIS, MET, and DTM models were examined by plotting standard deviation for each individual satellite based on daily data-to-model ratios covering the 1997–2004 period. While the statistics are determined using the actual satellite altitude, the data for each satellite are plotted at their average perigee altitude. Standard deviations are examined in Fig. 17. The data show a definite increase in model errors with altitude, as was also demonstrated by Bowman et al., 2006). The marked feature of Fig. 17 is that standard deviations for JB2006 are systematically lower than those for the other models at all altitudes. This advantage varies from about 2% (vs. J70 and MET) to 6.5% (vs. DTM) near 218 km to about 6% vs. all models near 600 km. The NRLMSIS, J70, and MET model errors all agree closely with altitude. The J70 values fall on those of MET up to about 550 km. The precision of the JB2006 model represents a

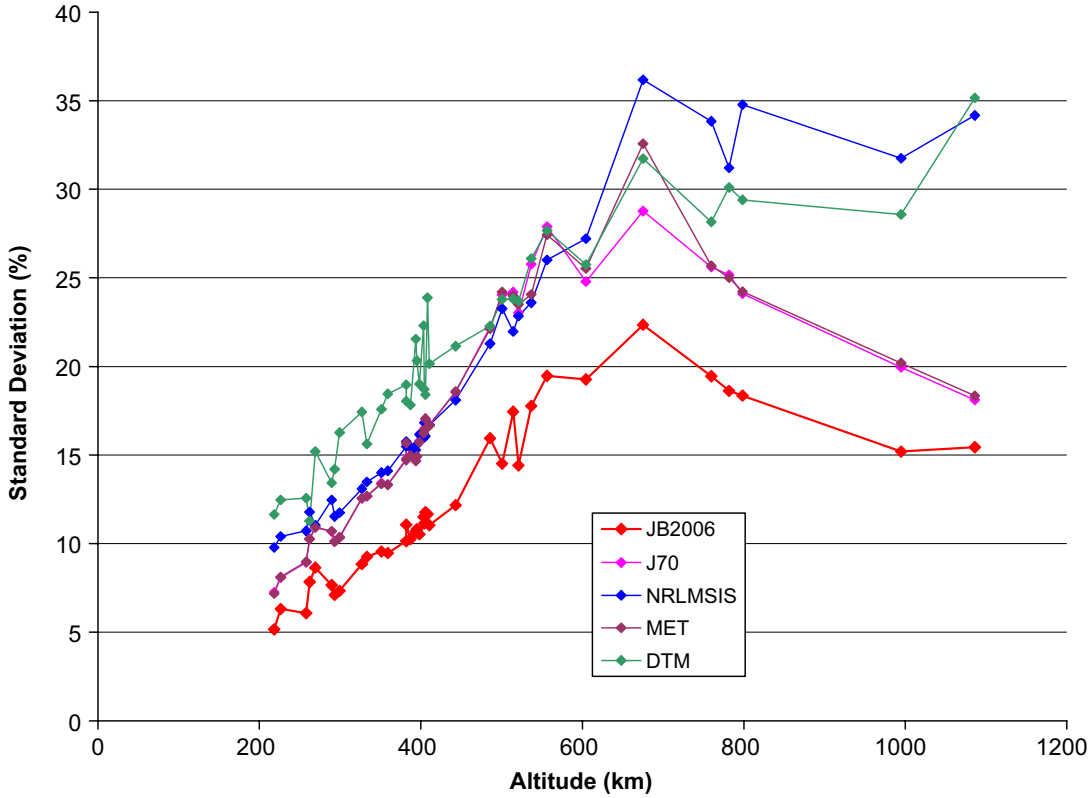

Fig. 17. Standard deviations of data-to-model ratios using 1997–2004 daily density data for JB2006, J70, NRLMSIS, MET, and DTM models vs. altitude.

significant improvement over all other empirical models.

8. Conclusions

Significant improvements in empirical density modeling have been obtained using the new JB2006 model incorporating new solar indices and a new semiannual variation equation. Solar indices representing the EUV and FUV atmospheric heating have been used to develop a new temperature equation to replace the standard Jacchia T_c equation. A new semiannual equation as a function of solar activity has replaced the standard Jacchia formulization, and new diurnal temperature correction equations have been added to the new model. Finally, density correction factors have been utilized to correct for the large Jacchia underestimation of the density at altitudes of 1000–4000 km. The new model, Jacchia–Bowman 2006 (JB2006), provides standard deviations of approximately 10% at 400 km, a significant decrease from 16% previously obtained using the Jacchia 70 model. A detailed description of the model, Fortran source code, new solar indices, and published papers describing the model equations can be obtained at the web site http://sol.spacenvironment.net/~jb2006/.

Acknowledgments

We would like to acknowledge the support of the Air Force Space Battlelab under the Sapphire Dragon initiative to improve the 72-h low earth orbit predictions.

References

Anselmo, L., Farinella, P., Milani, A., Nobili, A.M., 1983. Effects of the earth-reflected sunlight on the orbit of the LAGEOS satellite. Astronomy and Astrophysics 117, 3.

Barlier, F., Berger, C., Falin, J.L., Kockarts, G., Thullier, G., 1978. A thermospheric model based on satellite drag data. Annales de Geophysique 34, 451.

Berger, C., Biancale, R.R., Ill, M., Barlier, F., 1998. Improvement of the empirical thermospheric model, DTM: DTM-94-comparative review on various temporal variations and prospects in space Geodesy applications. Journal of Geodesy 72, 161.

Bowman, B.R., 2001. Atmospheric density variations at 1500–4000 km height determined from long term orbit perturbation analysis, AAS 2001-132. AAS/AIAA Spaceflight Mechanics Meeting, Santa Barbara, CA.

Bowman, B.R., 2002. True satellite ballistic coefficient determination for HASDM, AIAA-2002-4887. In: AIAA/AAS Astrodynamics Specialist Conference, Monterey, CA.

Bowman, B.R., 2004. The semiannual thermospheric density variation from 1970 to 2002 between 200–1100 km, AAS 2004-174. AAS/AIAA Spaceflight Mechanics Meeting, Maui, HI.

Bowman, B.R., Tobiska, W.K., 2006. Improvements in modeling thermospheric densities using new EUV and FUV solar indices, AAS 2006-237. AAS/AIAA Spaceflight Mechanics Meeting, Tampa, FL.

Bowman, B.R., Marcos, F.A., Kendra, M.J., 2004. A method for computing accurate daily atmospheric density values from satellite drag data, AAS 2004-179. AAS/AIAA Spaceflight Mechanics Meeting, Maui, HI.

Bowman, B.R., Tobiska, W.K., Marcos, F.A., 2006. A new empirical thermospheric density model JB2006 using new solar indices, AIAA 2006-6166. In: AIAA Astrodynamics Conference, Keystone, CO.

Bruinsma, S., Thullier, G., Barlier, F., 2003. The DTM-2000 empirical thermosphere model with new data assimilation and constraints at lower boundary: accuracy and properties. Journal of Atmospheric and Solar-Terrestrial Physics 65, 1053.

COSPAR International Reference Atmosphere, 1972. Compiled by the members of COSPAR Working Group 4. Akademie-Verlag, Berlin.

Hedin, A.E., 1983. A revised thermospheric model based on mass spectrometer and incoherent scatter data: MSIS-83. Journal of Geophysical Research 88, 10170.

Hedin, A.E., 1987. MSIS-86 thermospheric model. Journal of Geophysical Research 92, 4649.

Hedin, A.E., 1991. Extension of the MSIS thermosphere model into the middle and lower atmosphere. Journal of Geophysical Research 96, 1159–1172.

Hedin, A.E., Reber, C.A., Newton, G.P., Spencer, N.W., Brinton, H.C., Mayr, H.G., Potter, W.E., 1977. A global thermospheric model based on mass spectrometer and incoherent scatter data: MSIS 2. Composition. Journal of Geophysical Research 82, 2148.

Jacchia, L.G., 1970. New static models of the thermosphere and exosphere with empirical temperature profiles. Smithsonian Astrophysical Observatory Special Report 313.

Jacchia, L.G., 1971. Revised static models of the thermosphere and exosphere with empirical temperature profiles. Smithsonian Astrophysical Observatory Special Report 332.

Jacchia, L.G., 1977. Thermospheric temperature, density, and composition: new models. Smithsonian Astrophysical Observatory Special Report 375.

Jursa, A.S. (Ed.), 1985. Handbook of Geophysics and the Space Environment. Air Force Geophysics Laboratory, Air Force Systems Command, pp. 2-1–2-21.

King-Hele, D., 1964. Theory of Satellite Orbits in an Atmosphere. Butterworths, London.

Koskela, P.E., 1962. Orbital effects of solar radiation pressure on an earth satellite. Journal of the Astronautical Sciences 9, 71.

Marcos, F.A., 1990. Accuracy of atmospheric drag models at low satellite altitudes. Advances in Space Research 10, 417.

Marcos, F., Bowman, B.R., Sheehan, R.E., 2006. Accuracy of Earth's thermospheric neutral density models, AIAA 2006-6167. In: AIAA/AAS Astrodynamics Specialist Conference, Keystone, CO.

Owens, J., Vaughan, W., 2004. Semi-empirical thermospheric modeling: the new NASA Marshall engineering Thermosphere Model-Version 2.0 (MET-V2.0). 35th COSPAR Scientific Assembly, July 2004, Paris, France, p. 2708.

Paetzold, H.K., Zschorner, H., 1961. The structure of the upper atmosphere and its variations after satellite observations. In: Space Research II, 958. North-Holland Publishing Co., Amsterdam.

Picone, J.M., Hedin, A.E., Drob, D.P., Aikin, A.C., 2002. NRLMSISE-90 empirical model of the atmosphere: statistical comparisons and scientific issues. Journal of Geophysical Research 107 (A12), 1468.

Prior, E. J., 1971. Observed effects of Earth-reflected radiation and hydrogen drag on the orbital accelerations of balloon satellites. In: Symposium on the Use of Artificial Satellites for Geodesy, Washington, DC.

Rousseau, M., 1973. Densities deduced from perturbations at high altitudes. Planetary and Space Science 21, 1705.

Slowey, J. W., 1974. Radiation-pressure and air-drag effects on the orbit of the balloon satellite 1963 30D. Smithsonian Astrophysical Observatory Special Report 356.

Storz, M.F., et al., 2002. High Accuracy Satellite Drag Model (HASDM). AIAA 2002-4886. In: AIAA/AAS Astrodynamics Specialist Conference, Monterey, CA.

US Standard Atmosphere Supplements, 1966. ESSA, NASA, and US Air Force.

Viereck, R., Puga, L., McMullin, D., Judgem, D., Weber, M., Tobiska, W.K., 2001. The Mg II Index: a proxy for Solar EUV. Geophysical Research Letters 28 (7), 1342.